Article

Metallicity in Individual MMX Chains

Arrigo Calzolari, Simone S. Alexandre, Felix Zamora, and Rosa Di Felice

J. Am. Chem. Soc., **2008**, 130 (16), 5552-5562 • DOI: 10.1021/ja800358c • Publication Date (Web): 26 March 2008

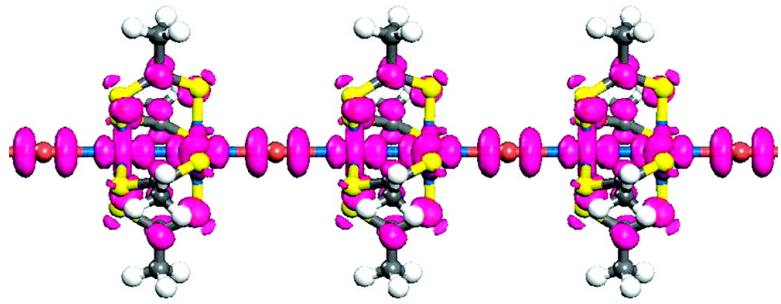

More About This Article

Additional resources and features associated with this article are available within the HTML version:

- Supporting Information
- Links to the 2 articles that cite this article, as of the time of this article download
- Access to high resolution figures
- Links to articles and content related to this article
- Copyright permission to reproduce figures and/or text from this article

View the Full Text HTML

J|A|C|S
ARTICLES

Published on Web 03/26/2008

Metallicity in Individual MMX Chains

Arrigo Calzolari,*,† Simone S. Alexandre,‡ Felix Zamora,§ and Rosa Di Felice*,†

National Center on nanoStructures and bioSystems at Surfaces (S3) of INFM-CNR, Via Campi 213/A, 41100 Modena, Italy, Departamento de Fisica, ICEx, Universidade Federal de Minas Gerais, C.P. 702, 30123-970-Belo Horizonte, MG, Brazil, and Departamento de Química Inorgánica C-VIII, Universidad Autónoma, ES-28049 Madrid, Spain

Received January 16, 2008; E-mail: arrigo.calzolari@unimore.it; rosa.difelice@unimore.it

Abstract: We present an ab initio study of the structural and electronic properties of the halogen-bridged MMX single polymer $[Pt_2(CH_3CS_2)_4I]_n$ and of various possible modifications of its sequence, in the framework of density functional theory. The computed band structure of the infinite regular polymer reveals a net metallic character; this evidence is compatible with the outcome of recent measurements done in the solid phase at room temperature. By taking the regular $[Pt_2(CH_3CS_2)_4I]_n$ polymer as our reference system, we analyzed the origin and the robustness of the metallic state along the chain with respect to a large set of geometrical and chemical perturbations of the subunits. In particular, we considered partial substitutions of the metal, halide, and dithiocarboxylate ligand subunits, as well as structural strain, defects, and magnetic effects. Our results demonstrate that the metallic character of single MMX chains is very resistant to a wide range of possible distortions that can occur in reality.

1. Introduction

The pursuit of ever denser and smaller electronic devices has fueled the investigation on novel materials at the nanoscale which should have good conduction properties and should be stable, easy to synthesize and manipulate, and able to self-assemble into supramolecular structures. Because of their high stability and good electronic properties,[1] carbon nanotubes are envisaged as promising candidates for molecular electronic devices. However, their intrinsic homogeneity and the difficulty in separating individual tubes from the synthesized bundles are hindering their widespread application in nanotechnology. Recently, coordination polymers, constituted of metal−organic building blocks, have been considered as alternative candidates for nanowires. In particular, the chalcogenide compounds, such as the molybdenum−sulfur−iodine[2] and the cadmium−mercaptopurinate[3] chains, have enough stability to isolate single polymers with controlled electronic properties. Among the classes of polymeric compounds with a potential fallout on nanotechnology, the MMX polymers are also attracting a growing research interest. The MMX polymers are quasi-one-dimensional (1D) chains constituted of repeated halogen-bridged mixed-valence binuclear metal complexes, in which the two metal atoms of each polymeric unit are linked pairwise by four ligands. Two types of polymers that differ for the ligand species are the main objects of investigation in the MMX class: (1) the *dta*-family $[M_2(dta)_4I]$ (M = Pt, Ni; *dta* = dithioacetate), characterized by neutral chains;[4−11] (2) the *pop*-family $A_4[Pt_2(pop)_4X]\cdot nH_2O$ (*pop* = $P_2O_5H_2^{2-}$; A = Li, K, Cs, NH_4; X = Cl, Br, I), characterized by anionic chains.[12−17]

† INFM-CNR.
‡ Universidade Federal de Minas Gerais.
§ Universidad Autónoma.

(1) Saito, R.; Dresslhauss, G.; Dresselhauss, M. *Physical Properties of Carbon Nanotubes*; Imperial College press: Bristol, 1998.
(2) (a) Remškar, M.; Mrzel, A.; Skraba, Z.; Jesih, A.; Ceh, M.; Demšar, J.; Stadelmann, P.; Lévy, F.; Mihailovic, D. *Science* **2001**, *292*, 479. (b) Zimina, A.; Eisebitt, S.; Freiwald, M.; Cramm, S.; Eberhardt, W.; Mrzel, A.; Mihailovic, D. *Nano Lett.* **2004**, *4*, 1749. (c) Vrbaniæ, D.; Remškar, M.; Jesih, A.; Mrzel, A.; Umek, P.; Ponikvar, M.; Janæar, B.; Meden, A.; Mihailovic, D. *Nanotechnology* **2004**, *15*, 635. (d) Meden, A.; Kodre, A.; Padežnik Gomilšek, J.; Arèon, I.; Vilfan, I.; Vrbanic, D.; Mrzel, A.; Mihailovic, D. *Nanotechnology* **2005**, *16*, 1578.
(3) (a) Olea, D.; Alexandre, S. S.; Amo-Ochoa, P.; Guijarro, A.; de Jesús, F.; Soler, J. M.; de Pablo, P. J.; Zamora, F.; Gómez-Herrero, J. *Adv. Mater.* **2005**, *17*, 1761. (b) Amo-Ochoa, P.; Rodríguez-Tapiador, M. I.; Castillo, O.; Olea, D.; Guijarro, A.; Alexandre, S. S.; Gómez-Herrero, J.; Zamora, F. *Inorg. Chem.* **2006**, *45*, 7642.
(4) Bellitto, C.; Flamini, A.; Gastaldi, L.; Scaramazza, L. *Inorg. Chem.* **1983**, *22*, 444.
(5) Bellitto, C.; Dessy, G.; Fares, V. *Inorg. Chem.* **1985**, *24*, 2815.
(6) Kitagawa, H.; Onodera, N.; Ahn, J.-S.; Mitani, T.; Toriumi, K.; Yamashita, M. *Synth. Met.* **1997**, *86*, 1931.
(7) Kitagawa, H.; Onodera, N.; Sonoyama, T.; Yamamoto, M.; Fukawa, T.; Mitani, T.; Seto, M.; Maeda, Y. *J. Am. Chem. Soc.* **1999**, *121*, 10068.
(8) Kitagawa, H.; Yamamoto, M.; Onodera, N.; Mitani, T. *Synth. Met.* **1999**, *103*, 2151.
(9) Kitagawa, H.; Sonoyama, T.; Mitani, T.; Seto, M.; Maeda, Y. *Synth. Met.* **1999**, *103*, 2159.
(10) Kitagawa, H.; Nakagami, S.; Mitani, T. *Synth. Met.* **2001**, *116*, 401.
(11) Otsubo, K.; Kobayashi, A.; Kitagawa, H.; Hedo, M.; Uwatoko, Y.; Sagayama, H.; Wakabayashi, Y.; Sawa, H. *J. Am. Chem. Soc.* **2006**, *128*, 8140.
(12) Yamashita, M; Miya, S.; Kawashima, T.; Manabe, T.; Sonoyama, T.; Kitagawa, H.; Mitani, T.; Okamoto, H.; Ikeda, R. *J. Am. Chem. Soc.* **1999**, *121*, 2321.
(13) Yamashita, M; Miya, S.; Kawashima, T.; Manabe, T.; Sonoyama, T.; Kitagawa, H.; Mitani, T. *Synth. Met.* **1999**, *103*, 2164.
(14) Kimura, N.; Ishimaru, S.; Kawashima, T.; Miya, S.; Manabe, T.; Yamashita, M.; Ikeda, R. *Synth. Met.* **2001**, *120*, 779.
(15) Matsuzaki, H.; Kishida, H.; Takizawa, K.; Yamashita, M.; Okamoto, H. *Synth. Met.* **2003**, *135–136*, 607.
(16) Wakabayashi, Y.; Kobayashi, A.; Sawa, H.; Ohsumi, H.; Ikeda, N.; Kitagawa, H. *J. Am. Chem. Soc.* **2006**, *128*, 6676.
(17) Yamashita, M.; Takaishi, S.; Kobayashi, A.; Kitagawa, H.; Matsuzaki, H.; Okamoto, H. *Coord. Chem. Rev.* **2006**, *250*, 2335.

 10.1021/ja800358c CCC: $40.75

Great interest has been generated in particular by the $Pt_2(dta)_4I$ complex, because it shows a clear metallic behavior under proper experimental conditions.[6,10,11] Although the mechanisms that rule electronic transport are not yet understood, the results of several measurements on $Pt_2(dta)_4I$ chains in the solid phase, done by different experimental techniques, show a metallic character at room temperature and the transition to a semiconductor state at low temperature ($T <$ 80 K). The metallicity of the system at room temperature is particularly appealing for nanoscale applications, because most devices operate at standard conditions. Peierls distortions in the chains are evoked as a possible origin of the metal−semiconductor transition.

The extraction of individual MMX chains from the solid-state phase would be of special interest because they may be used as 1D conductive elements in nanodevices, as well as to form hybrid supramolecular conductive aggregates with biological systems. Recently, we have isolated individual chains of $[Ru_2Br(\mu\text{-}O_2CEt)_4]_n$ on mica;[18] by following similar procedures, efforts are now concentrated to obtain individual $Pt_2(dta)_4I$ polymers. In our computational band-structure investigation, we focused solely on individual chains, and our results may trigger synthesis efforts toward the conditions for producing the most-promising nanowires from the point of view of electrical performance.

Despite the increasing interest in MMX compounds, only few studies addressed their theoretical modeling; most existing works[19−23] dealt with the description of the metal−semiconductor transition by means of ad hoc model Hamiltonians, which include a variety of possible interactions (e.g., electron−electron correlation, electron−phonon coupling, lattice distortion, etc.) in an effective way. The theoretical reports presented so far did not include the study of the 1D band structure, which is fundamental in the characterization of the conduction properties of the system. In this paper, we present a comprehensive ab initio atomistic investigation of the structural and electronic properties of several isolated and periodic $Pt_2(dta)_4I$ polymers, including a wide range of possible structural and chemical variations. Our results for the standard $Pt_2(dta)_4I$ polymer indicate that the uniform geometry that is observed at room temperature for the crystals is a metastable configuration also for the single chain. Its band structure unambiguously indicates a metallic behavior of the halogen-bridged chain. The characteristics and the origin of this metallicity are deeply analyzed through a comparative study of several variants, obtained by changing the assembling of the constituent subunits of the original polymer in viable different ways.

2. Method

We performed state-of-the-art electronic structure calculations based on density functional theory (DFT)[24] with the PBE[25] exchange-correlation functional, as implemented in the PWscf code.[26] The electron−ion interaction was described by ab initio ultrasoft pseudopotentials.[27] We explicitly included the semicore 5d (3d) shell of Pt (Ni) in the valence shell; only the valence electrons of the other species were explicitly treated. The electronic wave functions were expanded on a plane-wave basis set with an energy cutoff of 25 Ry; the completeness of this basis set is a posteriori witnessed by the fact that the optimized geometry of the $Pt_2(dta)_4I$ polymer is practically the same as the starting experimental one but also by other published works that report on different compounds containing the same or similar elements, including noble metals.[28] In addition, we tested the Pt and I pseudopotentials to reproduce correctly the bcc bulk phase of NaI and the fcc bulk phase of Pt crystals.

We simulated isolated quasi-1D MMX complexes by means of periodically repeated supercells. We arranged the chains in tetragonal supercells, with the long side along the axis of the polymer and with the length determined by the period of the polymer. The building block $M_2(dta)_4X$ is the monomeric unit, referred to in the following as M2-monomer. For a regular MMX polymer, the M−M and M−X distances, as well as the structure of the *dta* ligands, are the same in all the subsequent monomeric units. Thus, a single unit cell containing one M2-monomer is sufficient and was adopted by us (sections 3, 5, 6, and 7). If structural modifications (e.g., change of bond lengths between adjacent polymers, spin modifications, or introduction of defects) are applied, double (sections 3 and 4), quadruple, or 8-fold (section 8) cells are enforced, containing two, four, or eight M2-monomers, respectively. The number of M2-monomers included in the simulation supercell is specified in Table 1. In the directions perpendicular to the polymer axis, the equal sides were determined by the lateral size of the polymer plus a vacuum layer of ∼12 Å included in order to prevent spurious interactions between adjacent replicas. For Brillouin zone (BZ) integrations, 8, 4, 2, and 1 special k-points in the irreducible wedge of the 1D BZ (along the axis of the polymer) were used in single-cell, double-cell, quadruple-cell, and octuple-cell calculations.

The structure of each investigated polymer was relaxed before the computation of the band structure. The lattice parameter of the regular MMX polymers with different metals and halides was optimized by varying the longitudinal size of the single (monomeric) supercell and keeping the two transversal dimensions fixed, in order to maintain the lateral separation between adjacent replicas. For this optimization, we did total-energy and force calculations at a number of selected lattice parameters by relaxing all the atomic coordinates until the forces on all atoms were smaller than 300 meV/Å for each selected lattice constant. The optimal a_0 values (Table 1) derive from the quadratic fitting of the total energy profile as a function of the lattice parameter and estimation of the total energy minimum. We further checked the accuracy of the results and their independence from the choice of the basis set by optimizing the $Pt_2(dta)_4I$ structure also with the SIESTA code.[29]

The magnetic order of $Pt_2(dta)_4I$ and $Ni_2(dta)_4I$ polymers was investigated by using the local spin density (LSD) approximation. The effects of the electron−electron correlation, beyond standard

(18) Olea, D.; González-Prieto, R.; Priego, J. L.; Barral, M. C.; de Pablo, P. J.; Torres, M. R.; Gómez-Herrero, J.; Jiménez-Aparicio, R.; Zamora, F. *Chem. Commun.* **2007**, 1591–1593.
(19) Borshch, S. A.; Prassides, K.; Robert, V.; Solonenko, A. O. *J. Chem. Phys.* **1998**, *109*, 4562.
(20) Kuwabara, M.; Yonemitsu, K. *J. Mater. Chem.* **2001**, *11*, 2163.
(21) (a) Yamamoto, S. *Phys. Rev. B* **2001**, *63*, 125124. (b) Yamamoto, S. *Phys. Rev. B* **2002**, *66*, 165113.
(22) Nakano, S.; Kitagawa, Y.; Kawakami, T.; Yamaguchi, K. *Polyedron* **2003**, *22*, 2027.
(23) (a) Ohara, J.; Yamamoto, S. *Phys. Rev. B* **2004**, *70*, 115112. (b) Ohara, J.; Yamamoto, S. *J. Phys. Chem. Solids* **2005**, *66*, 1571. (c) Ohara, J.; Yamamoto, S. *Phys. Rev. B* **2006**, *73*, 045122.
(24) Dreizler, R. M.; Gross, E. K. U. *Density Functional Theory. An Approach to the Quantum Many-Body Problem*; Springer-Verlag: Berlin, 1990.
(25) Perdew, J. P.; Burke, K.; Ernzerhof, M. *Phys. Rev. Lett.* **1996**, *77*, 3865.
(26) Baroni, S.; Dal corso, A.; De Gironcoli, S.; Giannozzi, P. PWSCF; www.pwscf.org.
(27) Vanderbilt, D. *Phys. Rev. B* **1990**, *41*, 7892.
(28) Di Felice, R.; Selloni, A.; Molinari, E. *J. Phys. Chem. B* **2003**, *107*, 1151.
(29) Soler, J. M.; Artacho, E.; Gale, J. D.; García, A.; Junquera, J.; Ordejón, P.; Sanchéz-Portal, D. *J. Phys.: Condens. Matter* **2002**, *14*, 2745.

Table 1. Geometrical Parameters of the Investigated Polymers

	M2-monomers per cell	distances (Å)				angles (deg)		
		a_0[a]	d(M−M)[b]	d(M−X)[b]	⟨d(M−S)⟩[b]	(M−M−X)[c]	(M−X−M)[c]	⟨C−C−S−M⟩[c]
$Pt_2(dta)_4I$	1	8.64	2.73	2.95	2.41	179.9	180.0	168.7
zigzag	2	16.67	2.73	2.95	2.41	179.9	150.0	168.7
$Pt_2(dta)_4Cl$	1	8.11	2.73	2.70	2.36	179.9	180.0	169.2
ACP $\delta L = 0.23$ Å	2	17.28	2.76	3.00; 2.88	2.36	179.9	179.9	170.6
ACP + U $\delta L = 0.05$ Å	2	17.28	2.75	2.96; 2.96	2.36	189.0	180.0	170.7
$Ni_2(dta)_4I$	1	8.26	2.59	2.84	2.23	180.0	180.0	169.1
Oxy	1	8.64	2.75	2.94	2.35; 2.15(O)[d]	177.1	177.6	172.0; 169.9(O)[d]
CF_3	1	8.64	2.74	2.96	2.37	179.9	180.0	169.6
CN	1	8.64	2.73	2.95	2.39	180.0	179.9	169.2
I vacancy	8	63.82	2.73; 3.27	2.95	2.41	179.9	180.0	168.8
OH defect	4	33.34	2.73; 4.80	2.95; 2.95(O)[d]	2.41	179.9	180.0; 108.9(O)[d]	168.7

[a] a_0 is the lattice parameter of the 1D crystal in the longitudinal direction. The equilibrium value was computed only in selected cases, as described and motivated in the text. [b] d(M−M), d(M−X), and d(M−S) identify the metal−metal, metal−halogen, and metal−S distances, respectively. ⟨⟩ represents the mean value of a quantity over the considered unit cell. [c] (M−M−X) and (M−M−X) are the planar angles along the MMX chain. C−C−S−M is the torsion angle of the ligand with respect to the MMX chain. ⟨⟩ represents the mean value of a quantity over the considered unit cell. The double value for the Oxy polymer reflects the existence of two nonequivalent quantities in the cell. [d] (O) refers to the specific quantities with respect to the oxygen atom in the cell, instead of S or I.

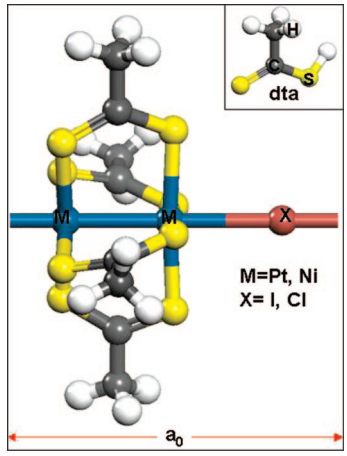

Figure 1. Optimized structure of the $M_2(dta)_4X$ M2-monomer, adopted as building block for the periodically repeated polymer. a_0 is the lattice parameter along the chain direction. The inset describes the atomic structure of the saturated dithioacetate (*dta*) ligand.

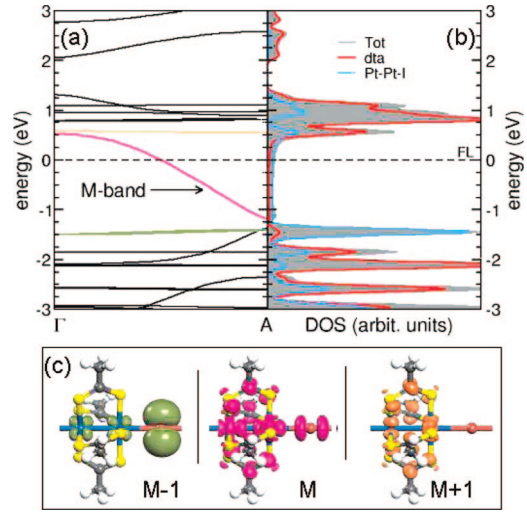

Figure 2. Band structure (a) and density of states (DOS) (b) of the isolated $Pt_2(dta)_4I$ polymer. The M band (pink line in panel a) is the metallic band that crosses the FL (dashed line, origin of the energy scale). The orange and the green solid lines identify nondispersive bands just above (M+1) and just below (M−1), respectively. The gray area in panel b represents the total DOS, and the solid blue and red lines represent the projections on the Pt−Pt−I chain and on *dta* groups, respectively. (c) Isosurface plots of electron states at the A point of the 1D BZ, which correspond to the three bands marked in panel a. The color code used for the isosurfaces is the same as in the band-structure diagram.

DFT, were taken into account through the inclusion of a local Hubbard potential U, within the GGA+U scheme implemented in the PWscf code.[30] Spin polarization was taken into account.

3. Reference Structure: $Pt_2(dta)_4I$ Polymer

We assume the $Pt_2(dta)_4I$ as the reference MMX prototype; its optimized structure is presented in Figure 1. It is characterized by the linear repetition of the metal−metal−halogen (Pt−Pt−I) atom sequence and by the helical arrangement of four dithioacetate ligands ($dta = CH_3CS_2^-$) around the central Pt−Pt−I axis.

As described in section 2, we optimized the lattice parameters and the atomic positions of the isolated perfect polymer, which is characterized by a unit cell that contains a single M2-monomer. The main structural results are reported in Table 1 and are in agreement with experimental X-ray data collected at room temperature.[10] In the relaxed configuration, the I atoms are bridge-bonded at the midpoint between two Pt atoms of adjacent M2-monomers. The central MMX chain is straight; it does not exhibit any vertical ripples or zigzag deformations.

From here on, we assume the regular optimized $Pt_2(dta)_4I$ polymer as the reference structure, to which we will compare various explored modifications.

The electronic structure analysis clearly shows the metallic nature of the $Pt_2(dta)_4I$ polymer. In fact, its band structure (Figure 2a) is characterized by a nondegenerate half-filled band that crosses the Fermi level (FL) along the Γ−A direction, which corresponds to the axis of the polymer. This is not surprising; it is the expected picture within the single-particle DFT description, given the odd number of electrons in the monomeric unit. The bandwidth [$\Delta E_M = E_M(\Gamma) - E_M(A)$] of this metallic band across the whole 1D BZ is 1.70 eV, as reported in Table 2. In order to get a better insight into the electronic structure and for further comparison with the other systems discussed later, we select and inspect in more detail a few bands near the Fermi energy. We label the selected bands M, M+1, M−1. M

(30) Coccocioni, M.; De Gironcoli, S. *Phys. Rev. B* **2005**, *71*, 035105.

Table 2. Electronic Structure Parameters of the Investigated Polymers: Bandwidths and Bandgaps

	ΔE_M[a,b] (eV)	ΔE_{M-1}[c] (eV)	ΔE_{M+1}[d] (eV)
$Pt_2(dta)_4I$	1.70	0.20	0.06
$Pt_2(dta)_4I$ ($U = 3$)	1.72	0.14	0.37
$Pt_2(dta)_4I$ ($U = 6$)	1.51	0.15	0.49
zigzag	1.21[e]	0.67[e]	0.06
Pt_2I	2.99		
$Pt_2(dta)_4Cl$	1.54	0.86[f]	0.14
$Ni_2(dta)_4I$	0.83	0.41[f]	0.41
$Ni_2(dta)_4I$ ($U = 3$)	0.77	0.43	0.55
$Ni_2(dta)_4I$ ($U = 6$)	0.69	0.44	0.68
Oxy	1.82	0.18	0.13
CF_3	1.73	0.09	0.13
CN	1.57	0.10	−0.02

[a] ΔE_M is the bandwidth of the M bands across the 1D BZ: $\Delta E_M = E_M(\Gamma) - E_M(A)$. [b] Band labeling (M, M−1, M+1) follows Figure 2. [c] ΔE_{M-1} is the energy separation between bands M and M−1 at the edge of the 1D BZ: $\Delta E_{M-1} = E_M(A) - E_{M-1}(A)$. [d] ΔE_{M-1} is the energy separation between bands M and M+1 at the center of the 1D BZ: $\Delta E_{M+1} = E_{M+1}(\Gamma) - E_M(\Gamma)$. [e] Because of the BZ folding, the value is calculated at the Γ point. [f] Note that, because of a band crossing, the M−1 band (green in band-structure plots) is not the first band below the M band at the edge of the 1D BZ (point A). On the basis of symmetry considerations, we maintain this label for a direct comparison with the other systems.

(hereafter associated to the color pink) is the metallic band. M+1 (orange) and M−1 (green) are the nondispersive bands just above and below the M band, respectively. The M−1 band is doubly degenerate and fully occupied, whereas the M+1 band is nondegenerate and empty. We define $\Delta E_{M-1} = E_M(A) - E_{M-1}(A)$, the energy separation between bands M and M−1 at the edge of the BZ (point A in Figure 2a), and $\Delta E_{M+1} = E_{M+1}(\Gamma) - E_M(\Gamma)$, the energy gap between bands M and M+1 at the center of the BZ (point Γ); the corresponding values are reported in Table 2.

In the theoretical model presented so far by other groups,[19–21] the metallic band of the polymer is ascribed to the hybridization among the d_{z^2} orbitals of Pt atoms and the pz orbital of the halogen atoms, thus reducing the complexity of the electronic structure to a two-band system. Our atomistic approach reveals instead a more complex scenario. In Figure 2b, we report the density of states (DOS) of the chain, which reproduces the trend defined in the band structure. To understand the origin of the selected bands, we project the total DOS (shaded area) onto the atomic states localized on each of the two subsystems in the polymer, namely, the Pt−Pt−I chain (blue line) and the lateral *dta* ligands (red line). We note that both subsystems contribute to the DOS at the FL, denoting the importance of the *dta* functional groups for the overall conductivity of the chain. We rationalize also the different characteristics of the M−1 and M+1 bands. The spectral weight of the M−1 band is mainly due to the Pt_2I states, whereas that of the M+1 band is primarily due to the *dta* fragments. In fact, the first peak below the FL is dominated by the blue line, and the first peak above the FL is dominated by the red line.

The isosurface plots of the single particle orbitals (Figure 2c) confirm this interpretation. Indeed, the doubly degenerate M−1 band corresponds to two linear combinations of weak interacting d_{xz} (d_{yz}) states of Pt with the p_x (p_y) states of I (those in the direction perpendicular to the chain), with no notable coupling with the ligands. The central panel of Figure 2c shows the mixed character of the M band: the antibonding σ-like contribution deriving from the d_{z^2}-p_z hybridization, delocalized along the Pt−Pt−I chain, and the π-like contribution distributed over the CS_2 fragments of the *dta* ligands. Finally, the M+1 band results from the mixing of d states of Pt atoms with sp orbitals of the chelator groups, excluding the halogen states.

The specific bonding path of the $Pt_2(dta)_4I$ polymer leads to a formal +5 oxidation state for each Pt−Pt pair (i.e., +4 due to the four *dta* ligands and +1 due to the I atom), which corresponds to a formal +2.5 charge state per Pt atom or equivalently to one unpaired spin per Pt−Pt pair. In our DFT calculations, the net charge transfer from Pt atoms to the rest of the environment is symmetric and smaller than the formal one. Analysis of the Lowdin charges indicates that the I atom is negatively charged ($\delta q(I) = -0.46$ e), and the Pt atoms are positively charged ($\delta q(Pt) = +1.09$ e). Even though the calculated values are smaller than the formal ones, the presence of itinerant (unbalanced) spins might induce a magnetic behavior in the system. We tackled this issue by decoupling the spin degrees of freedom within the LSD framework. We took into account four starting configurations in a double cell (two M2-monomers per cell) associated to different spin orientations at the Pt sites, namely:

(a) (↑↑,↑↑)

(b) (↑↓,↑↓)

(c) (↑↓,↓↑)

(d) (↑↑,↓↓)

Systems (a) and (b) reproduce the ferro- and antiferromagnetic alignment, respectively; systems (c) and (d) are instead non-magnetic. We calculated the corresponding electronic structures by keeping the atoms fixed in the previously optimized geometry and checking a posteriori that the inclusion of the spin degrees of freedom does not induce additional forces on the atoms. The four systems converged to the same paramagnetic (zero magnetization) configuration, having the same total energy (within $\Delta E_{tot} = 10^{-5}$ eV/cell). The resulting electronic structures exactly reproduce, for each spin component, the electronic structure shown in Figure 2. Thus, our results predict a non-magnetic character of the $Pt_2(dta)_4I$ chains, in agreement with experimental findings at room temperature.[7,31]

The presence of oxidized $Pt^{+\delta q}$ atoms (i.e., partially empty 5d shell) and the low dimensionality of the polymer, however, invoke the rise of strong electron−electron (e−e) correlation effects, as proposed for other Pt-based quasi-1D chains.[32,33] Thus, we also performed spin-polarized calculations beyond the LSD approximation. In order to account for e−e interactions beyond the mean-field treatment of DFT calculations, we introduced a local Hubbard potential U on Pt sites, within a standard LSD+U approach, to investigate the modifications deriving from inclusion of two different values of the parameter U, namely $U = 3$ and 6 eV, previously adopted for similar systems.[32,33] In both cases, we started with the optimized structure (one M2-monomer per cell) described above, and we let the system relax in the presence of the potential U, within the LSD approach, in order to deal with singly occupied electronic states. Despite the inclusion of the Hubbard potential,

(31) Tanaka, H.; Kuroda, S.; Yamashita, T.; Mitsumi, M.; Toriumi, K. *J. Phys. Soc. Jpn.* **2003**, *72*, 2169.
(32) Ferretti, A.; Calzolari, A.; Di Felice, R.; Manghi, F.; Caldas, M. J.; Buongiorno Nardelli, M.; Molinari, E. *Phys. Rev. Lett.* **2005**, *94*, 116802.
(33) Ferretti, A.; Calzolari, A.; Di Felice, R.; Manghi, M. *Phys. Rev. B.* **2005**, *72*, 125114.
(34) (a) Dal Corso, A.; Mosca, A. *Phys. Rev. B* **2005**, *71*, 115106. (b) Dal Corso, A.; Smogunov, A.; Tosatti, E. *Phys. Rev. B* **2006**, *74*, 045429.

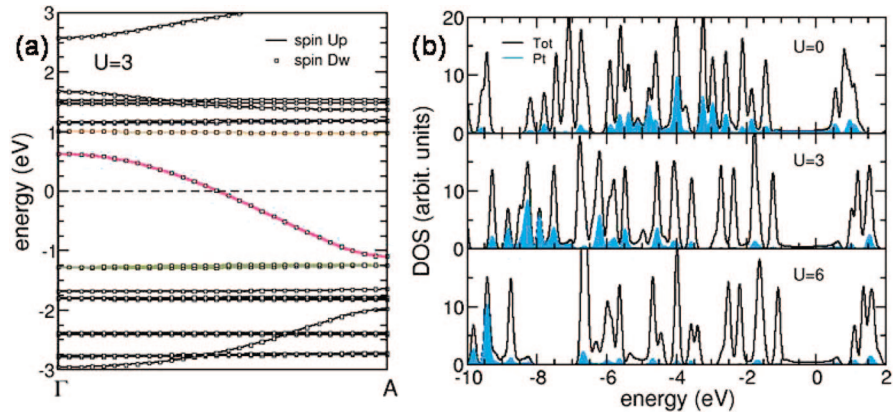

Figure 3. (a) Spin-resolved GGA+U band structure of the $Pt_2(dta)_4I$ polymer for $U = 3$ eV. The color code is the same as in Figure 2, solid (dotted) curves are the spin-up (spin-down) bands. (b) Spin-up DOS of the polymer for selected values of the Hubbard potential $U = 0$, 3, and 6 eV. Black lines identify the total DOS, and the shaded areas are the DOS projections onto the Pt atomic orbitals. The zero energy references are set to the FL of each calculation.

the resulting geometry and electronic structure do not present notable modifications with respect to the uncorrelated case. The spin-up (solid) and spin-down (dashed) band structure for the $U = 3$ eV case is presented in Figure 3a; a similar diagram can be obtained also for $U = 6$ eV (not shown). The inclusion of the on-site correlation does not introduce any further spin polarization in the system. We can identify the selected M, M+1, and M−1 bands, which have the same symmetries and degeneracies as in the mean-field system. Increasing the correlation potential to $U = 6$ eV, the dispersion of the M band, ΔE_M, slightly decreases, and the energy separations ΔE_{M-1} and ΔE_{M+1} increase, as reported in Table 2. However, the system maintains the pristine metallic behavior and does not undergo any Mott−Hubbard transition. The persistence of the metallicity in the correlated systems is analyzed in Figure 3b by comparing the spin-up DOS curves computed with different values of the parameter U (similar behavior holds for spin-down). Because the Hubbard potential is active only at the Pt sites, we explicitly draw the projected density of states (p-DOS) on the Pt atoms (blue area). As expected, the presence of the Hubbard potential tends to localize the d states of Pt. The effect of the localization is the quench of the Pt d component at the FL, with the consequent opening of a partial gap in the Pt projected spectra, to an extent that depends on the strength of U. This localization mechanism is not enough to change the conduction properties of the polymer; the M band component due to *dta* ligands (red line in Figure 2b) does not suffer the effects of the on-site e−e correlation and maintains the metallic behavior of the chain.

It has been discussed in theoretical studies that the inclusion of the spin−orbit interaction might affect the electronic and magnetic properties of heavy open-shell elements (such as Pt). For both Pt fcc-bulk[34a] and monatomic Pt chains,[34b] it has been shown that the relativistic effects may change the degeneracy and the dispersion of a few energy bands. However, in the specific case of MMX polymers, we believe that such effects (if any) may yield only minor modifications to the presented results; that is, they do not change the qualitative description of the ground state of these wires. The spin−orbit effect is expected to change, for instance, the numerical values of the effective mass or the mobility of the charge carriers in these polymers, to be compared with the experimental data. However, such a strict quantitative comparison goes beyond the purpose of the present work and is also hindered by the lack of conductivity measurements for single chains. Furthermore, we note from our results that the M band that crosses the FL, which determines the conductive behavior of the polymers, is not due to the simple Pt−Pt state interaction (as in ref 34b) but is the result of the complex interplay of the metal atoms with the halogens and the bridged groups, for which the relativistic interaction may reasonably be ignored.

4. Structural Distortions

Here, we take into account a few configurations that break the uniform periodicity of the $Pt_2(dta)_4I$ polymer. We are interested in the effects induced by the inclusion of linear distortions. This issue is also related to the understanding of the possible origin of the semiconducting behavior observed in the solid-state phase at low temperature ($T < 80$ K). So far, the metal−semiconductor transition observed in crystals was attributed to several causes, such as structural distortions, e−e and electron−phonon interactions, solitons, solid-state effects, defects, and so forth.[6,7,10,22,23] We do not intend to directly address this question, because we are interested in the properties of individual MMX chains. Thus, we limit our investigation to understanding the effects induced on the electronic structure of the isolated polymer by the inclusion, in the 1D system, of some physical features that are proposed to be responsible for the metal−insulator transition in the solid-state case.

On the basis of the possible oxidation states of the $Pt_2(dta)_4I$ polymer, different types of valence structures have been proposed, depending on the charge states of the metal atoms, average valence (AV), charge density wave (CDW), charge polarization (CP), and alternate charge polarization (ACP) states, namely:

(1) (AV) $M^{+2.5}$—$M^{+2.5}$—X—$M^{+2.5}$—$M^{+2.5}$—X—

(2) (CDW) M^{+2}—M^{+2}—X—M^{+3}—M^{+3}—X—

(3) (CP) M^{+2}—M^{+3}—X—M^{+2}—M^{+3}—X—

(4) (ACP) M^{+2}—M^{+3}—X—M^{+3}—M^{+2}—X—

Hyphens of different length in the above scheme are used to indicate different bond lengths; note that only the metal−halogen distance changes. The valence states expressed as M^{+2} and M^{+3} should be more accurately presented as $M^{(2+\delta)+}$ and $M^{(3-\delta)+}$. Model (1) corresponds to the undimerized configuration described in section 3. The valence structures (2) and (3) involve

a displacement (δL) of each halogen atom from the midpoint between two M2-monomers. In the ACP configuration, there is a δL displacement of the M-M units toward the central halogen atom (that remains at the midpoint between adjacent M2-monomers), which leads to the formation of two inequivalent M-X-M sequences, precisely M^{+3}—X—M^{+3} and M^{+2}—X—M^{+2}. Models (1) and (2) have uniform charge distribution within a single $Pt_2(dta)_4I$ M2-monomer, whereas models (3) and (4) have an intrinsic charge polarization. Recent experimental results (X-ray,[10] ^{129}I Mossbauer,[9] and IR and Raman spectroscopy[8]) indicate that the valence ordering structure of this compound at temperatures below 80 K should be the ACP state, even though a conclusive statement can not yet be given.

The four valence structures were simulated in a double cell with a longitudinal size equal to that of two consecutive cells of the perfect $Pt_2(dta)_4I$ polymer (Table 2). We first considered the AV case, checking the effect of the repetition of the structural optimization in a double cell that contains two M2-monomers, without any further lattice relaxation. The optimized geometry does not indicate any additional dimerization or energy gain, confirming that the undistorted configuration is a metastable phase for the system. Even in the case of a double-cell configuration, constituted of two M2-monomers rotated by 90° along the polymer axis, no dimerization is obtained spontaneously. The rotated system has practically the same total energy ($\Delta E_{tot} = 1.6$ meV/M2-monomer), revealing a negligible coupling between the *dta* groups of adjacent M2-monomers.[35] In both cases, the electronic structure replicates that of the reference structure with a single M2-monomer per cell, except for the obvious folding of the BZ, which causes the crossing between the FL and the M band to be at the BZ edge. We also considered the case of a nonlinear geometry including a rippling angle between adjacent M2-monomers along the chain direction. The zigzag structure is obtained by bending the two M2-monomers in a double cell by 30°, while keeping the Pt−Pt and Pt−I distances as in the linear chain (see Table 1). The system is still metallic with only minor modifications of the band structure properties (see Table 2). Even though these results are not conclusive on the metallic character of a generically disordered MMX wire, as it might be in solution and/or when deposited on a surface, they seem to suggest that the metallicity is not dramatically affected by an angular distortion.

In the case of CDW, CP, and ACP structures, we started with the atomic displacement $\delta L = 0.05$ Å, which amounts to ∼2% (∼3%) of the Pt−Pt (Pt−I) bond length. We let all the systems fully relax. The CDW, CP, and ACP optimized structures have the same total energy (within the accuracy of our DFT calculations) as the AV optimized structure. Namely, we cannot resolve the energy gain of alternative motifs with respect to the ideal chain. The 2−3% distortion imposed on the ACP starting geometry results, after relaxation, in a tiny residual contraction of 0.5−0.7%, which is practically equivalent to the undimerized reference AV motif. We interpret this finding as the indication that Peierls distortions induced by an amount of axial strain that is in the elastic regime (2−3%) are extremely weak. The electronic structure is essentially unaffected by the structural distortion; we expect that the tiny gap of 25 meV[36] that opens at the edge of the BZ would not change the effective behavior of the chain as a metal in transport experiments at room temperature and under applied electric fields, with an effective M band having a bandwidth of $\Delta E_M = 1.85$ eV. Distorted structures may instead explain the insulating behavior observed in several experiments at low temperature, although it remains true that DFT total-energy and force calculations are affected by an error on the total energy that makes them not predictive about the energy gain upon small elastic strain.

We conclude that these slight axial deformations should not compromise the metallic character of these chains in applications at room temperature. The AV phase represents the local minimum of the potential energy surface for the MMX polymer where all the strained structures sampled in this section converge. However, this does not exclude that other distorted configurations might be more stable than the regular AV one. In order to check this hypothesis, we strongly increased the δL displacement in the ACP configuration, taking $\delta L = 0.23$ Å, namely, ∼9% of the Pt−I bond length. The optimized geometry that we obtained starting from this condition maintains a Peierls distortion; the atomic distortion is reduced with respect to the starting constraint, the long Pt−I bonds being about 4% larger than the short ones. This trend cannot be ascribed to the choice of the plane-wave basis set, because similar results have been obtained with a localized basis set implemented in the SIESTA code.

The electronic structure of the highly distorted configuration (Figure 4) shows remarkable new features. The system is no longer metallic and has a finite bandgap, $E_g = 0.11$ eV, definitely larger than that at room temperature beyond any error due to smearing.[36] The original M band is split into two subbands (labeled H and L in Figure 4a), which correspond to two orthogonal highest occupied molecular orbital (HOMO) and lowest unoccupied molecular orbital (LUMO) states (Figure 4b). The isosurface plots of the single-particle orbitals highlight on one hand the nonequivalence of the two halogen sites and, on the other hand, the reduction of the metal−*dta* interaction.

Finally, we considered the simultaneous effect of the structural distortion, the spin polarization, and the electronic correlation on the electronic structure of the polymer. We prepared the system (labeled ACP+U) in the slightly distorted ACP geometry, with $\delta L = 0.05$ Å and two M2-monomers per cell, in order to move the system from the undistorted metastable AV phase. We included also a $U = 6$ eV potential on Pt atoms, in order to enhance the possible effects of correlation on the structural and electronic properties of the system. After the total-energy and force relaxation process within the local spin density framework, the polymer maintains the key characteristics of the reference regular $Pt_2(dta)_4I$ chain. The joint effect of atomic deformation and electron correlation does not cause further axial distortions (Table 1), restoring the almost midpoint position (within 0.02 Å) of the halogen atom with respect to the neighbor Pt atoms. The effects on the electronic structure are also reduced; the system maintains its paramagnetic character (zero magnetic polarization), which corresponds to the spin-up and spin-down

(35) The reciprocal orientation of the lateral *dta* groups does not modify the overall properties of the isolated polymers, but it may have important effects in the crystalline structure because of the steric packing.

(36) This result may in part be affected by our use of a finite temperature for the smearing of the Fermi function. We tested the outcome by using various values of such a temperature, down to 10 meV, and found no difference. This indicates that the error on the determination of the band gap (beyond the intrinsic DFT error) should be smaller than 10 meV, hence not relevant for electrical measurements at room temperature.

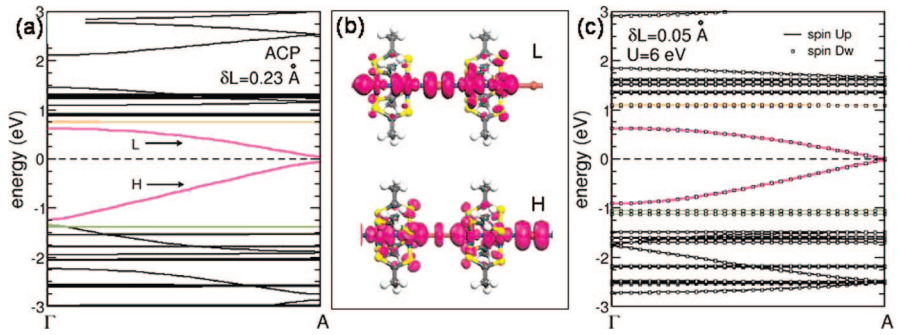

Figure 4. (a) Band structure of $Pt_2(dta)_4I$ polymer, in the case of a large structural distortion ($\delta L = 0.23$ Å) along the polymer axis, according to the ACP model. (b) Isosurface plots of the HOMO (H) and of the LUMO (L) at the A point of the 1D BZ, belonging to the pink-colored bands of panel a. (c) Spin-resolved band structure of $Pt_2(dta)_4I$ polymer in the simultaneous case of a structural distortion ($\delta L = 0.05$ Å) and electron correlation ($U = 6$ eV). Both unit cells include two M2-monomers. Band colors follow those defined in Figure 2. The origin of the energy scales is set at the FL (dashed line). Solid (dotted) curves denote spin-up (spin-down)

spectra being completely degenerate in energy (Figure 4c). There is a very small gap, $E_g = 0.025$ eV, at the edge of the BZ, smaller than that obtained for the large distorted ACP structure presented so far. The energy gap is of the order of the room temperature energy ($E_{RT} \approx 0.025$ eV). Thus, this is likely to result in an effective metallic system with a gapless density of states, as already discussed above. We note also that the applied $U = 6$ eV is a huge potential, higher than realistic ones.

We can conclude that our results suggest that only extreme distortions, which likely lead to plastic deformations, are able to drive the system into the semiconducting state, whereas distortions that remain in the elastic range systematically reproduce the metallic-like character. We cannot resolve, on the basis of the energy balance, whether the uniform or the distorted configuration is more favorable. Both configurations are characterized by similar total energies that differ only by 30 meV/M2-dimer and are therefore both viable. Peierls distortions cannot be excluded as the origin of the metal−insulator transition, but our calculations are not conclusive on this point; indeed, other effects typical of the crystal phase (lattice size and arrangement between neighboring chains in the lattice) can be responsible or co-responsible for the observed transition.

5. Role of the Ligand Subunit

In the previous sections, we showed how the metallic behavior of the $Pt_2(dta)_4I$ polymer is the result of interactions among the three subunits of the system: the metal−metal pair, the halogen atom, and the four *dta* lateral groups. Here, we analyze the effects on the band structure induced by the selective dropping of ligand subunits.

We computed the electronic structure of the simplified chain, constituted only of the Pt−Pt−I sequence (labeled also Pt_2I chain), without the dithiocarboxylate ligands. We maintained the atoms fixed in the same cell exploited to describe the perfect polymer, with one M2-monomer in the simulation cell.

The absence of the ligands strongly modifies the charge distribution along the chain; the formal charge state should be $\delta q = +0.5$ e per Pt atom. The model chain is still metallic (Figure 5), but its electronic structure is dramatically different from that of the $Pt_2(dta)_4I$ polymer. Two weakly dispersive bands cross the FL. However, the character of these bands is not related to the M band of the reference polymer; it is rather more similar to the M−1 band (except for the absence of the *dta* contribution). We also notice the presence of a very dispersive band (bandwidth of 2.99 eV), which is partially

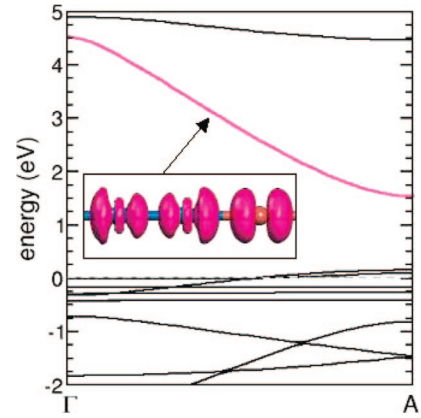

Figure 5. Band structure of the model Pt_2I chain (without ligand groups). The origin of the energy scale is set at the FL. Inset: isosurface plot of the M electron state at the A point of the 1D BZ.

reminiscent of the d_{z^2}-p_z M band of the $Pt_2(dta)_4I$ system (see inset of Figure 5). However, this band is completely empty in the Pt_2I chain model; its lowest edge is 1.54 eV above the FL at point A. We conclude that the strong coupling among the Pt atoms and the *dta* ligands affects both the character and the occupation of the electronic states near the FL in MMX chains. This conclusion implies that changes of the specific coupling between the subunits modify the overall conduction properties of the complex. The importance of the ligands is in line with what was previously found in MX polymers,[37] although it was discussed there in a different context, namely, for the influence on dimerization along the chain rather than for showing the orbital hybridization. In both MMX and MX chains, the ligands attract charge away from the linear axis, thus affecting the electronic character.

6. Metal and Halogen Modifications

In this section, we explore the properties of other MMX sequences, similar to the $Pt_2(dta)_4I$ polymer but obtained by substituting either the metal or the halogen atoms with isoelectronic atoms. We focus on the $Pt_2(dta)_4Cl$ and the $Ni_2(dta)_4I$ complexes. The former includes Cl instead of I, and the latter includes Ni instead of Pt. In both cases, the replacement of an element along the chain skeleton changes the bonding lengths

(37) Alouani, M.; Albers, R. C.; Wills, J. M.; Springborg, M. *Phys. Rev. Lett.* **1992**, *69*, 3104.

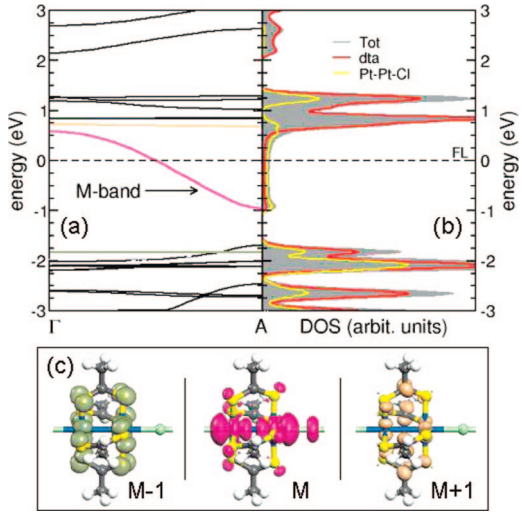

Figure 6. Band structure (a), DOS (b), and selected isosurface plots of electron orbitals (c) for the $Pt_2(dta)_4Cl$ polymer. Colors and symbols follow those defined in Figure 2. The origin of the energy scale is set at the FL (dashed line).

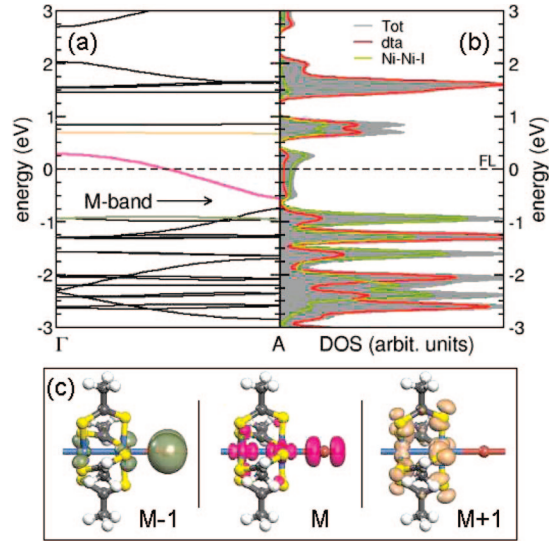

Figure 7. Band structure (a), DOS (b), and selected isosurface plots of electron orbitals (c) for the $Ni_2(dta)_4I$ polymer. Colors and symbols follow those defined in Figure 2. The origin of the energy scale is set at the FL (dashed line).

and the periodicity of the 1D chain. We optimized the lattice parameter by following the procedure described in section 2 for the perfect polymer (one M2-monomer/cell).

6.1. $Pt_2(dta)_4Cl$ Polymer. The $Pt_2(dta)_4Cl$ chains have been proposed but not yet synthesized. Because Pt ions usually have a larger hybridization with iodides than with chloride or bromide composites, the I-based compounds are expected to be more stable than the other halogen-bridged polymers. On the other hand, Cl has been largely exploited in similar charged MMX polymers, with different lateral *pop* groups.[17,23,37] The optimized structure obtained by relaxing the cell size (see Table 1) has a lattice parameter shorter (−6%) than that of $Pt_2(dta)_4I$. This modification is to be ascribed to the contraction of the Pt−Cl distance, which is coherent with the smaller dimension of Cl with respect to I. The compound maintains a uniform and linear configuration with the halogen atom placed at the midpoint between consecutive dimers.

Figure 6 shows the structure and density of states. The polymer is metallic and presents electronic features similar to those of the iodide compound; the M, M+1, and M−1 bands are easily recognizable. We notice, however, a 10% reduction of the bandwidth ΔE_M of the metallic band, together with a huge increase of the energy gap ΔE_{M-1} at the edge A of the BZ. In Figure 6b, we decoupled the contributions to the DOS due to the Pt−Pt−Cl chain (yellow line) and to the *dta* fragments (red line). The M band contains both components, and the M+1 band is dominated by the *dta* one, as for $Pt_2(dta)_4I$. This is also confirmed by the analysis of the Kohn−Sham states in Figure 6c. Different is the case of the M−1 band, which loses the component deriving from the p states of the halogen and gains contribution from the *dta* groups (compare Figures 2c and 6c). This feature, along with the shrinking of the M bandwidth, indicates smaller metal−halogen hybridization, which is coherent with the more localized nature of the 3p orbitals of Cl with respect to the 5p orbitals of I. This rationalizes a posteriori the fact that it is easier to synthesize I- instead of Cl-based MMX polymers.

6.2. $Ni_2(dta)_4I$ Polymer. The structure of the Ni-based MMX polymers has been studied from the experimental point of view,[5,9] but only very few theoretical models have been reported for bulk phases.[22,23] In our work, we optimized the structure and characterized the electronic ground state of the $Ni_2(dta)_4I$ chains, for comparison with the Pt-based ones.

The smaller covalent radius of Ni atoms causes a reduction of the lattice parameter (−4%) as well as of the bonding lengths with respect to those of $Pt_2(dta)_4I$ (see Table 1). The final effect is a scaling down of the polymer along its axis, without any further conformational modification (e.g., no dimerization and no rippling).

The analysis of the electronic structure (Figure 7) shows that the system is metallic and very similar to the $Pt_2(dta)_4I$ polymer. We identify a dispersive M band that crosses the FL. This band has the same symmetry as that of the reference polymer (compare Figures 7c and 2c) and derives from several contributions that include Ni, I, S, and C atoms, as shown in the projected density of states in Figure 7b. In the $Ni_2(dta)_4I$ polymer, however, the M bandwidth is $\Delta E_M = 0.83$ eV, which is almost half of that for the $Pt_2(dta)_4I$ polymer; this is probably due to the greater localization of the 3d states of Ni with respect to the 5d states of Pt. This is confirmed by the Lowdin charges $\delta q(Ni) = +0.67$ e and $\delta q(I) = -0.34$ e, which are more similar to the isolated atomic ones. We also note that the M band is isolated because of the larger ΔE_{M+1} and ΔE_{M-1} gaps. The other features are very similar to those of the Pt reference.

We inspected the effects of the spin coupling and of the strong e−e correlation, typical of Ni atoms. For this purpose, we did spin-polarized calculations of the electronic structure of the polymer in the double cell, assuming the starting spin configurations (a−d) described in section 3. The results reproduce the Pt cases; all systems converged to the same ground-state nonmagnetic configuration (zero magnetization), with the same total energy.

The picture remains unchanged also after the inclusion of the Hubbard potential on the Ni sites. Two values for the U potential (U = 3 and 6 eV) were taken into account in the LSD+U scheme. The results follow the trend described for the Pt polymer; the correlated systems maintain a metallic behavior, because the chain−ligand mixing hinders the opening of an energy gap at the FL. The introduction of the e−e correlation splits only the Ni-derived component of the DOS, leading to a

progressive reduction of the M bandwidth when U is increased (see Table 2).

The investigation of metal and halogen substitution thus reveals that the metallic character of the MMX polymers is very robust against this type of changes, although in principle, one could expect major changes, especially when inserting a very correlated metal such as Ni that has extremely localized d states. On the other hand, this does not exclude the possible existence of other nonmetallic MMX chains based on different metals and different halogens.

We note that a more pronounced difference is revealed between Ni-based and Pt-based MX polymers constituted by an alternated sequence of metal and halogen atoms, where different mechanisms explain the dimerization and consequent insulating character (charge-transfer in NiX and Mott−Hubbard in PtX).[39] It was already pointed out that MMX polymers are profoundly dissimilar because of the minor role of electronic correlations due to the vicinity of two metal atoms and the direct metal−metal coupling.[7] This explains the viability of metallic chains, in which only differences in bandwidths and bandgaps are found between Ni and Pt. For the insulating phase (studied here only for Pt and not for Ni), differences between Ni and Pt identical to those found in MX polymers can be expected, namely, smaller bond contractions for Ni than for Pt and different mechanisms for the metal−insulator transition.

7. Ligand Modifications

MMX polymers were synthesized with several dithioacetate derivatives (RCS_2^-), with variable-length lateral chains (R = ethylene, *n*-butyl, *n*-pentyl, and *n*-propyl groups).[7,11,16,32,38,40–43] The lateral size of the ligand groups does not change significantly the electronic properties but may affect the intrapolymer interactions in the crystalline phase. Because we are interested in the properties of the individual chains, we decided to consider other kinds of chemical modifications of the original *dta* group that may, in principle, influence the electronic and conduction properties of the single chain.

In one case (labeled Oxy), we substituted one S atom per M2-monomer with an O atom, as shown in Figure 8a. This configuration cannot be classified simply as a substitutional defect, because it is periodically repeated along the polymer, but it has to be considered as another model polymer, which is helpful to characterize the role of S atoms on the structural and electronic properties. O and S are isoelectronic. However, O being more electronegative, it may unbalance the charge distribution along the chain. The presence of O atoms makes the two Pt atoms in each M2-monomer nonequivalent. We name them in the following Pt_{SO} (bonded to O) and Pt_S (non-bonded to O).

We relaxed the forces on all the atoms by a single-cell calculation. The optimized structure presents notable distortions

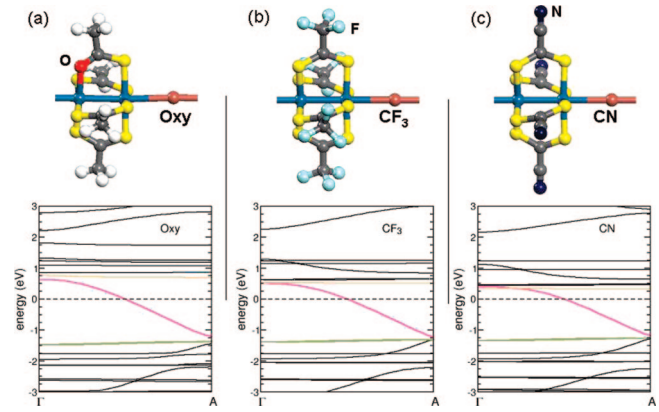

Figure 8. Atomic structure (upper panels) and corresponding band structure (bottom panels) of Pt−Pt−I polymers with chemically modified ligand groups. (a) Substitution of one of the four S atoms with an O atom; (b) substitution of all the terminal CH_3 groups with CF_3 groups; and (c) substitution of all the terminal CH_3 groups with CN groups. Band colors follow those defined in Figure 2. The origin of the energy scale is set at the FL (dashed line).

of the chelator fragment that includes the O atom (see Table 1). The contraction of the Pt−O and O−C distances induces a partial bending of the attached group and an out-of-line displacement of the Pt atoms, which slightly ripple the chain. Despite the geometrical modifications, the electronic structure does not undergo dramatic changes (Figure 8a). The system is metallic with the M-band states delocalized through Pt atoms and *dta* ligands. The M band has a bandwidth $\Delta E_M = 1.82$ eV, that is, 7% larger than that of the reference polymer. The calculated Lowdin charges, $\delta q(Pt_{SO}) = +1.15$ e, $\delta q(Pt_S) = +1.08$ e, $\delta q(I) = -0.45$ e, $\delta q(O) = -0.44$ e, and $\langle \delta q(S) \rangle = -0.01$ e, confirm that the O atom attracts more electronic charge than each S atom does. This charge transfer involves primarily the C atoms of the fragment and only slightly the bonded Pt_{SO} ion. Note also that the δq values of Pt and I atoms are practically the same as those in the pristine polymer.

The second modification we considered consists in substituting all the external methyl groups CH_3 with CF_3 groups (Figure 8b). After the structural optimization, no remarkable distortions are detected (see Table 1). The electronic structure (Figure 8b) does not change too much with respect to the reference case; the system is metallic, and the M bandwidth is very similar to that of the reference polymer (Table 2). Despite the strong electron-acceptor characteristic of the CF_3 group, its inclusion in the polymer does not modify the intrinsic band structure of the starting system; that is, it does not act as a chemical doping. This is in agreement with the metallic nature of the system that tends to screen the effects of the charge transfer toward the lateral groups. The calculated Lowdin charges confirm that the electron accumulation on the F atoms ($<\delta q(F)> = -0.21$ e) mainly derives from the C atoms of the CF_3 groups ($\langle \delta q(C_F) \rangle = +0.84$ e), whereas the charge state on the other species remains unaltered with respect to the reference $Pt_2(dta)_4I$ polymer.

Finally, we considered the substitution of the methyl groups with cyano groups CN (Figure 8c). The atomic relaxation does not reveal any notable modifications in the geometry and in the electronic structure. The results are summarized in Tables 1 and 2, respectively. Figure 8c shows that the metallic character of the system persists, with a narrower M bandwidth (−8%). We also note a band crossing between the M and M+1 bands in the $\Gamma-A$ direction, which may be ascribed to a downward

(38) Mitsumi, M.; Kitamura, K.; Morinaga, A.; Ozawa, Y.; Kobayashi, M.; Toriumi, K.; Iso, Y.; Kitagawa, H.; Mitani, T. *Angew. Chem., Int. Ed.* **2002**, *41*, 2767.
(39) Springborg, M.; Dong, Y. *Metallic chains/Chains of Atoms*; Elsevier: Amsterdam, 2007.
(40) Saito, K.; Ikeuchi, S.; Nakazawa, Y.; Sato, A.; Mitsumi, M.; Yamashita, T.; Toriumi, K.; Sorai, M. *J. Phys. Chem. B* **2005**, *109*, 2956.
(41) Ikeuchi, S.; Saito, K.; Nakazawa, Y.; Mitsumi, M.; Toriumi, K.; Sorai, M. *J. Phys. Chem. B* **2004**, *108*, 387.
(42) Tanaka, H.; Hasegawa, Y.; Ito, H.; Kuroda, S.; Yamashita, T.; Mitsumi, M.; Toriumi, K. *Synth. Met.* **2005**, *152*, 141.
(43) Mitsumi, M.; Murase, T.; Kishida, H.; Yoshinari, T.; Ozawa, Y.; Toriumi, K.; Soniyama, T.; Kitagawa, H.; Mitani, T. *J. Am. Chem. Soc.* **2001**, *123*, 11179.

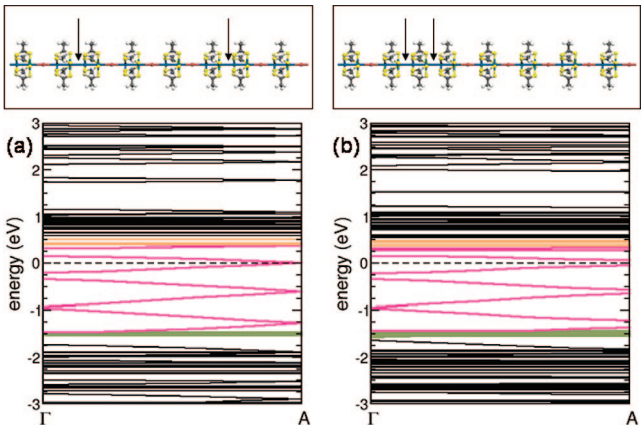

Figure 9. Atomic structure (upper panels) and corresponding band structure (bottom panels) of the $Pt_2(dta)_4I$ polymer in the presence of structural defects that consist of I vacancies (25%). An 8-fold supercell was employed, with adjacent M2-monomers rotated by 90° with respect to each other relative to the longitudinal axis. Band colors follow those defined in Figure 2. The origin of the energy scale is set at the FL (dashed line). (a) Secluded I vacancies: the FL crosses the M band and the system is metallic. (b) Segregated I vacancies: a small gap (120 meV) opens at point A.

shift of the conduction bands, caused by the electrostatic effects imposed by the strong electron-donor behavior of cyano groups.

The three functional cases presented in this section underline the persistence of the chain metallicity upon various designed chemical modifications of the *dta* group. This enforces the importance of the joint Pt−I and Pt−S interactions for the overall conduction properties of the chain and opens the way to a large range of possible functionalizations of the outermost groups for envisaged formation of complex molecular architectures (polymer coating, anchoring of biomolecules, etc.).

8. Point and Substitutional Defects

In the previous sections, we considered selected modifications of the polymer subunits that do not involve changes of the periodicity. Here, we take into account the effects induced by the inclusion of punctual and substitutional defects that may occur in the synthesis procedures.

8.1 Point Defects: I Vacancy. We inspected the role of isolated defects obtained with 25% of I vacancies. To do this within our periodic supercell approach, we considered a larger unit cell containing eight M2-monomers, in two of which the I atom was subtracted (see Figure 9, top panels). In principle, this amount of vacancies could be investigated by a 4-monomer supercell. However, we adopted a larger one in order to access two different configurations characterized by dilution (Figure 9a, separated vacancies) and segregation (Figure 9b, adjacent vacancies).

The starting I-vacancy configurations were built by taking the Pt−I distance (2.73 Å) from the reference structure (section 3), and the Pt−Pt distance in each M2-monomer (3.27 Å) was optimized in an infinite halogen-free $Pt_2(dta)_4$ chain. Any two consecutive M2-monomers are rotated by 90° relative to the longitudinal axis. We did not further relax the structure, but we checked that the forces per atom were negligible.

The band structure of the systems is plotted in Figure 9. The M band is 8-folded because of the multiplicity of M2-monomer components in the unit cell. A small gap within the M manifold is opened at the Γ point for both secluded and segregated vacancies. However, this gap is internal to the M manifold, and it is not by itself sufficient to destroy the metallic character of the polymer. The band diagram in Figure 9a shows that in the secluded I-vacancy polymer, the FL crosses one branch of the M manifold. Thus, this I-vacancy polymer, despite the high defect concentration considered here, cannot be responsible for a metal−insulator transition (although, in principle, it could be responsible for this transition on the basis of electron counting). However, the band diagram in Figure 9b shows that segregated vacancies are indeed able to induce a metal−insulator transition. In fact, a small gap of 120 meV opens at the BZ edge (A point). Although this gap value is rather small, it is responsible for a breakage of the metallic character. Thus, even if the electron states around the FL remain delocalized along the polymer axis and efficient charge transfer may occur, the formation of segregated halogen vacancies represents a possible mechanism for destroying the coherence of the conductivity.

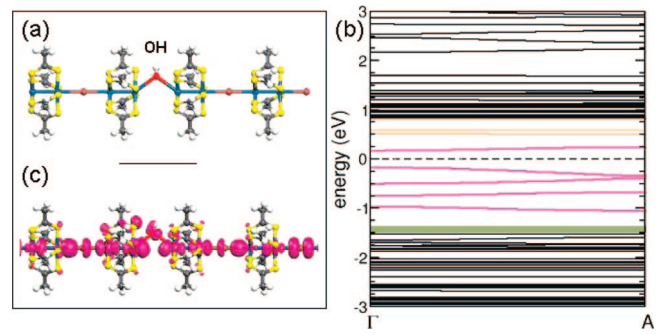

Figure 10. Atomic structure (a), band structure (b), and isosurface plot of the highest occupied orbital at the A point of the 1D BZ (c) for the $Pt_2(dta)_4I$ polymer in the presence of OH substitutional defects (25%). A quadruple supercell was employed, with adjacent M2-monomers rotated by 90° with respect to each other relative to the longitudinal axis. Band colors follow those defined in Figure 2. The origin of the energy scale is set at the FL (dashed line).

8.2. Substitutional Defects: OH. The chemical modifications described in section 7 deal with the changes in the *dta* groups that surround the metal−metal−halogen chain. From an experimental point of view, these examples would require different synthesis procedures that intrinsically modify the nature of the polymer. Therefore, the previous modifications lead to different kinds of polymers; that is, they cannot be considered defects for the $Pt_2(dta)_4I$ system. On the contrary, we report here on the substitution of a single halogen atom with a OH molecule that may experimentally occur during the standard synthesis of the $Pt_2(dta)_4I$ polymer. The ultimate system that we would like to simulate is the isolated defect; in order to achieve this configuration by means of our periodic supercell approach, we studied the effect of one OH substitution in a quadruple cell containing four $Pt_2(dat)_4I$ building blocks, as shown in Figure 10a. On the basis of experimental results for similar polymers,[3] we fixed the Pt−O−Pt angle at 109°. The Pt−O distance was arbitrarily taken as equal to the Pt−I bond length, namely, 2.95 Å.[44]

Subsequent M2-monomers are rotated by 90° in order to reduce the steric interactions between the *dta* residues near the OH defect. Because of the computational effort required to simulate this configuration, we did not relax the lattice parameter

(44) We are aware that this value is too large for a Pt−O distance to occur in a realistic compound. However, our results indicate that it is enough to realize bonding between O and Pt, thus grasping all the relevant features to identify the qualitative features of the defect. The precise quantitative aspects are beyond the scope of our analysis and hindered by the lack of reliable experimental data.

and the atomic coordinates. The exact evaluation of the polymer geometry in the presence of one isolated OH defect goes beyond the aim of this work. We just wish to check whether such a substitutional defect may be responsible for breaking the chain and changing the metallic character.

The electronic structure of the system is shown in Figure 10b. The chain is indeed no longer metallic and has a direct gap $E_g = 0.34$ eV at the Γ point. In the region near the gap, it is possible to recognize a set of bands (pink) that are reminiscent of the metallic M band of the periodic chain. The 4-fold multiplicity is not clear because of mixing of M-like orbitals with p orbitals of the O atom. Figure 10c shows the isosurface plot of the highest occupied orbital at the A point; it is evidently related to the M character (compare to Figure 2c), except at the OH site where the delocalized d_{z^2}-p_z orbital is interrupted. We note also a reduction of the metal−ligand coupling. These features lead to the breaking and the flattening of the ideally 4-folded M band.

9. Concluding Remarks

We presented a detailed analysis of the structural and electronic properties of MMX polymers from a first-principles study. Our DFT results show that the uniform structure (AV) represents a metastable configuration for the system. The chain has a metallic behavior that is in agreement with the experimental findings at room temperature in the crystalline phase. The metallic M band that characterizes the system is the result of simultaneous hybridization of metal orbitals with the halogen and with the *dta* ligands. The observed metallicity is very robust: we deeply investigated the robustness of the metallic character by using different numerical codes (i.e., different basis sets), as well as by studying auxiliary systems obtained by decomposing and reassembling the different subunits that constitute MMX polymers. Whereas some of the explored alterations and tests were purposely designed to break the metallic behavior, others were just meant to understand whether the metallic mechanism remains the same in different chemical conditions. We find that only very strong external perturbations, such as a huge compressive distortion,[36] a substitutional defect, or segregated vacancies, manage to destroy the metallic character of the isolated polymer.

The persistence of the metallic behavior of the individual polymers is particularly attractive for their possible nanoscale applications, for example, the fabrication of molecular devices that should operate at room temperature.

Acknowledgment. We thank Julio Gomez and José Soler for fruitful discussions. This work was funded by the EC through project DNA-based Nanodevices (Contract FP6-029192), CNPq and CAPES (Brazil), the Regional Laboratory of Emilia Romagna Nanofaber, and Ministerio de Educación y Ciencia of Spain (NAN2004-09183-C10-06). Access to the CINECA supercomputing facilities was granted by INFM-CNR.

JA800358C